The Corrosion Resistance of Hard Anodised EN AW 7075 T6 Alloy

KUSMIČ, D.; KLAKURKOVÁ, L.; JULIŠ, M.; GEJDOŠ, P.; VILIŠ, J.; ČECH, O.

ECS Transaction
2021, vol. 105, iss. 1, pp. 329-337

ISSN: 1938-6737

DOI: http://dx.doi.org/10.1149/10501.0329ecst

Accepted manuscript

Citation:

KUSMIČ, D.; KLAKURKOVÁ, L.; JULIŠ, M.; GEJDOŠ, P.; VILIŠ, J.; ČECH, O. (2021). The Corrosion Resistance of Hard Anodised EN AW 7075 T6 Alloy. *ECS Transaction*, 105(1), 329–337. https://doi.org/10.1149/10501.0329ecst

The Corrosion Resistance of Hard Anodized EN AW 7075 T6 Alloy

D. Kusmič[a], L. Klakurková[b], M. Juliš[b] P. Gejdoš[b], J. Viliš[a], O. Čech[c]

[a] Department of Mechanical Engineering, University of Defence, Brno, Czech Republic,
[b] Research Group RG 1-06, CEITEC Brno University of Technology, Brno, Czech Republic
[c] Department of Electrical and Electronic Technology, Brno University of Technology, Brno, Czech Republic

In this paper, commercially cold-rolled and artificial aged EN AW 7075 T6 alloy has been used. To ensure increased corrosion resistance, surface hardness, scratching resistance, and aesthetic features were this aluminium alloy subsequently hard anodized and hot-water sealed (AC-A). The hard anodizing and sealing process increased surface hardness up to 304±13 HV, from an initial surface hardness of 194±3 HV. Also, the microhardness of the anodized layer and bulk material has been documented. Scanning electron microscopy (SEM) was used for microstructure and trapped precipitates investigation in the 42.9±1.4 thick formed anodized layer investigation. The corrosion properties of the T6 treated (AC) and hard anodized and sealed (AC-A) EN AW 7075 alloy were evaluated using the anodic potentiodynamic polarization tests (PPT) in a neutral 2.5% NaCl deaerated solution. The corrosion rate CR (mm/y) decreased approx. 39-times for the hard anodized and sealed EN AW 7075 alloy (AC-A), associated with the shift of the E_{corr} (mV) to more positive values, degreased Icorr (μA) and increased Rp (Ohm) values compared to the artificial aged (AC) alloy. Additionally using the laser confocal microscopy, the pitting was evaluated, and the pitting coefficient was calculated as well.

1 Introduction

The aluminium alloys (AA) are generally attractive thanks to comprehensive properties, such as ductility, toughness, fatigue resistance, low density and high specific strength comparable with high strength steels (1, 2). Thank to mentioned properties is the AA EN AW 7075 widely used in many engineering applications with the intention of weight reduction, especially in the aircraft, automotive or arms industry (3, 4). However, the use of EN AW 7075 mainly limits its poor tribological properties due to its low surface hardness and susceptibility to adhesion. These shortcomings are to some extent eliminated by precipitation hardening (artificial ageing). The EN AW 7075 alloy (7000 series) is a so-called cold-curable or naturally curable alloy at room temperature. The 7000 series alloys are very suitable for use in structures where welding is required and where no further heat treatment (solution annealing and hardening) can be performed after welding. Immediately after welding, the strength in the transition zone is low but increases with natural curing. Finally, 90% of the original strength can be achieved (5). These thermal processes are associated with structural changes associated with the concentration and distribution of

intermetallics and strengthening particles leading to increased sensitivity to localized corrosion, such as intergranular corrosion, exfoliation and stress corrosion cracking, compared to EN AW 6082, for example (5, 6). To suppress the susceptibility of the above-mentioned types of corrosion attack, alternative methods of heat treatment of these types of AA have been investigated and developed (7, 8, 9).

To achieve satisfactory corrosion resistance in the aerospace industry, the EN AW 7075 alloy is mostly pure aluminium plated, hard anodized or painted. According to the anodizing process condition and additive technologies can by even the mechanical properties of the anodized oxide layer, and/or modified by adding PTFE suspension to the working electrolyte improved (10). Increased mechanical and corrosion properties are achieved by the application of the hard anodizing process on the AA. The anodizing process takes place most often in the H_2SO_4 working electrolyte with an electrolyte temperature in the range of -5 °C up to 5 °C to ensure increased surface hardness (350-400 HV). The formed anodic layers on the AA are formed by a thick outer porous layer and by a thin non-porous structure (called a barrier layer) on the interface porous outer layer and the substrate (11, 12). The faster dissolving of intermetallic particles than of the matrix is the reason for creation of a heterogeneous (porous) outer anodic layer. The porous outer anodic layer tends to be sensitive to aggressive environments and mechanical stress (13, 14). To increase the corrosion resistance of anodized AA the sealing procedure is essential. The sealing takes place most often in boiling solutions (hot-sealing) as in boiling deionized water, in metal salt solutions, or under lowered temperatures (82-88 °C), or low temperatures (28-32 °C, Cold Sealing). The hexavalent chromium-containing solutions used for anodising and sealing confer excellent corrosion resistance to the aluminium alloys. Due to their toxicity, chromium-free anodising and sealing baths are therefore more attractive in industry applications (13).

In this work, EN AW 7075 alloy commercially treated to T6 and hard anodized in H_2SO_4 electrolyte, and hot sealed in deionized water was studied. Light microscopy, electron microscopy (SEM and EDX) and laser confocal (LCF) microscopy were used to study the aluminium alloy and the hard-anodized oxide layer. The corrosion evaluation was performed using the anodic potentiodynamic polarization tests (PPT) in a neutral 2.5% NaCl deaerated solution.

Experimental and Results

For this study, the EN AW 7075 alloy (AA) was chosen with chemical composition (in wt.%): 5.61 Zn, 2.3 Mg, 1.7 Cu, 0.39 Fe, 0.2 Cr, 0.13 Mn, 0.12 Si, 0.023Ti (verified by the Q4 Tasman spectrometer). The AA samples were supplied in a commercially T6 state (rolled, solution heat-treatment and artificially ageing, usually to the maximum strength). The heat treatment consisted of solution-treatment at 470 °C for 1 h (quenching in water) and ageing at 120 °C for 24 h to achieve the maximal tensile strength of 545-559.8 MPa (5, 9). The investigated EN AW 7075 was commercially hard anodized in H_2SO_4 electrolyte, and hot sealed in deionized water to achieve improved tribological and corrosion properties. Specimens were prepared with dimensions of 90 x 50 x 5 mm for microstructural and chemical analysis. Prepared specimens (artificial aged, anodized and hot-sealed) were cut and rounded into a final sample of diameter 15 mm, needed for the internal diameter of the potentiostat working electrode holder (without additional polishing the surface).

Characterization and microstructure

Figure 1 shows the microstructure of artificial aged AA (T6) on a cross-sectional metallographically prepared specimen mounted in the self-curing denture base acrylic resin. The cut specimens were ground with abrasive papers, polished by 3 μm and 1 μm diamond suspension and finally polished with colloidal SiO_2, rinsed with acetone, degreased with distilled water, dried in the air, finally etched in FUSS etchant (0.7 vol. % HF + 2.4 vol % HCl + 0.8 vol % HNO_3 + distilled water). The main alloying elements, in the studied AA, are Zn, Mg and Cu. The precipitation sequence of the studied alloy can be described as a supersaturated solid solution (α) → GP zone → metastable η' → stable η intermetallic (8). The most strengthening intermetallics formed in the artificial aged AA are metastable $\eta'(MgZn_2)$ and stable η ($MgZn_2$) intermetallics situated in the grain-boundary and in the matrix. The $MgZn_2$ intermetallics in the range of a few nanometers up to 270 nm are dispersed in the grains of solid solution and on the grain boundaries. $Al_{12}Mg_2Cr$ intermetallics with increased size (0.5–30 μm), and additionally Al_7Cu_2Fe, Al_3Fe, Mg_2Si, Al_2CuMg and $MgZn_2$ intermetallics with various size and density were also documented by other authors (15, 16, 17). The EDS analysis also revealed more complex intermetallics based on Al-Fe-Si-Cr-Cu-Mn-Zn elements, as documented in Figure 2.

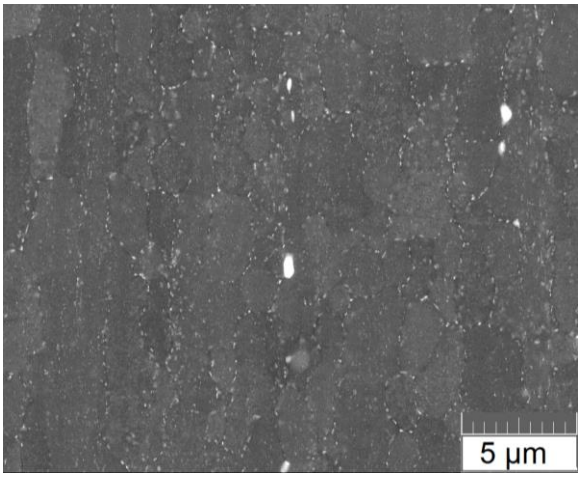

Figure 1. Microstructure of artificial aged EN AW 7075 alloy

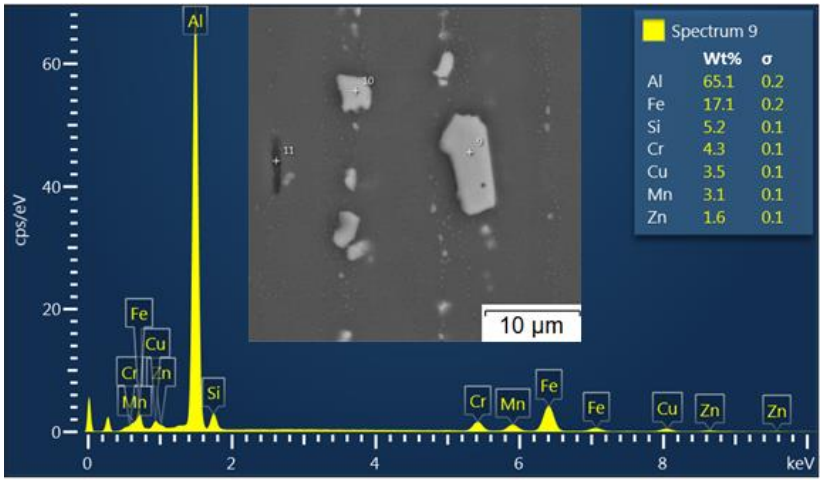

Figure 2. Al-Fe-Si-Cr-Cu-Mn-Zn based intermetallics (EDS, SEM LIRA3 TESCAN)

Table I lists the surface characteristics (surface hardness, microhardness and anodized layer thickness) of artificial aged AA (marked as AC) and hard anodized and hot-sealed AA (marked as AC-A). The surface hardness was measured on originally prepared AA samples (AC and AC-A samples) using the Vickers Hardness Tester LV 800AT and the microhardness measurements were performed on cross-sectional metallographically prepared specimens.

TABLE I. Surface hardness, microhardness, anodized layer thickness

EN AW 7075	Surface hardness (HV)	Microhardness (HV0,1)	Anodized layer (µm)
AC	194±3	179±4	-
AC-A	304±13	329±60	42.9±1.4

The surface hardness of the AC-A sample increased to 304±13 HV, from an initial surface hardness of 194±3 HV (AC sample). The surface hardness of the AC-C sample is generally slightly lowered after the hot-sealing process. The microhardness measurements on prepared cross-sectional metallographic specimens indicated an increase in the variance of microhardness values in the hard anodized layer, generally caused by layer imperfection of columnar anodized layer (like cavities, pores, dissolved or undissolved intermetallic particles and cracks) as documented in Fig. 3, which have been already discussed by other authors (10, 18).

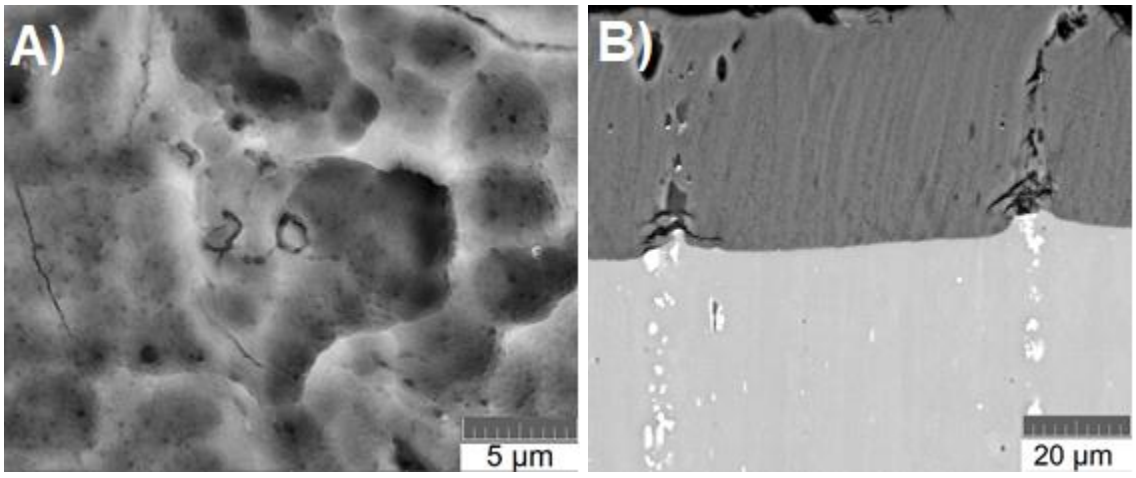

Figure 3. SEM (BSE) of hard anodized layer – A) surface morphology, B) cross-sectional morphology (SEM-BSE LIRA3 TESCAN)

Corrosion Behavior

The anodic potentiodynamic polarization test (PPT) was performed to artificial aged AA (AC sample) and hard-anodized and sealed AA (AC–A sample) on prepared samples with a final diameter of 15 mm, decreased in ethanol prior testing. For this purpose the Cyclic Potentiodynamic Polarization measuring method was used (according to ASTM-61 standard) with following parameters: sweep speed dE/dt = 0.166 mV/s, Ei = -0.25 V, EL = 2 V, Ip = 25 mA, E range (-2 V; 2 V) at ambient temperature in neutral deaerated 2.5% NaCl solution. The measured area of the surface of samples was 0.865 cm^2. As the counter electrode was used the Supersaturated Calomel Electrode (SCE). To the recorded curves in Figure 5 was the Tafel extrapolation method was applied and the corrosion rates CR (mm/y) were calculated.

The polarization curves of the artificial aged AA (AC sample) and to hard-anodized and sealed AA (AC–A sample) are plotted in Figure 5. The measured corrosion potentials, corrosion currents and polarization resistance values are summarized in Table II.

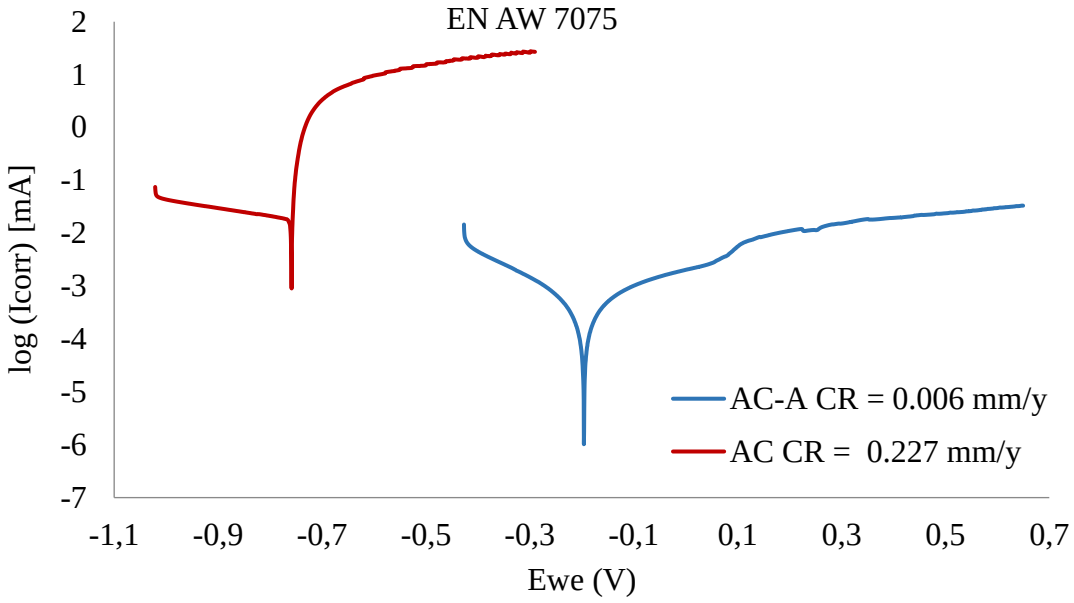

Figure 5. PPT curves of artificial aged (AC) and hard-anodized and sealed EN AW 7075 alloy (Biologic SP 150 device, EC-Lab V11.10. software)

TABLE II. The PPT results

EN AW 7075	E_{corr} (mV vs. SCE)	I_{corr} (µA)	Rp (Ohm)	CR (mm/y)
AC	-776.55	19.30	371	0.227
AC-A	-202.79	0.49	85 331	0.006

The Tafel extrapolation method on the recorded polarization curves was used by the EC-Lab V11.10 software. As plotted in Figure 5, the PPT curves demonstrate the beneficial effect of hard anodizing with consequent hot sealing in deionized water. The initial value of E_{corr} = - 776.55 mV for the AC sample is shifted to a more positive value E_{corr} = - 202.79 mV for the AC-A sample. However, the E_{corr} (mV) is not sufficient to evaluate the corrosion behaviour. It is well known, that corrosion is controlled by the corrosion rate, which is linear with total anodic current I_{corr} (µA) or with total current density i_{corr} (µA /cm^2) by Faraday´s law, corresponding to the anodic and cathodic kinetics. The Tafels constants βa (mV) for anodic branch and βc (mV) for cathodic branch were determined from the polarization curves (Figure 5). The beneficial effect of hard anodized and sealed AA is also documented by a simultaneous decrease in total corrosion currents to the value of I_{corr} = 0.49 µA from initial I_{corr} = 19.3 µA for AC sample and a significant increase in polarization resistance value to R_p = 85 331 Ohm from initial R_p = 371 Ohm (AC sample), as summarized in Table II. A crucial role play presented intermetallic particles in the artificial aged EN AW 7075 T6 alloy and also trapped intermetallics in the hard anodized layer. These intermetallics of different particle size and density are characterized by different electrochemistry to the α solid solution, as investigated by M. K. Cavanaugh et al (17). Part of these intermetallics are polarized anodically ($MgZn_2$, Mg_2Si) or cathodically

(Al_7Cu_2Fe, Al_3Fe and Al_2CuMg) to the α solid solution having a different interaction with the α solid solution. The anodically polarized particles are expected to dissolve anodically. The cathodically polarized particles, supporting mainly the oxygen reduction, are responsible for dissolving of the α solid solution in their vicinity. These particles are supporting the local cathodic corrosion, developing pitting and then increased fatigue cracking sensitivity. So the calculated corrosion rate for the AC sample reached the value CR = 0.227 mm/y and for the AC-A sample only CR = 0.006 mm/y.

Surface evaluation after corrosion testing

Surfaces of artificial aged and hard anodized AA samples were additionally documented after anodic potentiodynamic polarization tests, as documented in Figure 6. Pitting was evaluated using laser confocal microscopy LEXT OLS 3000 and pitting factor (PF) was calculated, as summarized in Table III. The pitting factor was calculated according to standard ISO 11463 as a ratio of the deepest pit to the average depth of 10 measured pits. The pitting factor of value 1 indicates general corrosion and with the increased value of the pitting factor, the pitting corrosion is more prominent.

TABLE III. The pitting evaluation and pitting factor

EN AW 7075	**Pitting depth**			**PF (-)**
	Min. (μm)	Max. (μm)	Ø (μm)	
AC	20.67	56.96	41.8	1.36
AC-A	14.6	16.3	15.6	1.01
AC-A before PPT	11.6	15.5	13.8	-

A significant difference between AC and AC-A samples was documented after PPT (see Figure 6 A and B and Table III.). The average pitting depth for the AC sample reached 41.8 μm and calculated PF = 1.36. As documented the hard-anodizing significantly reduced pitting. The surfaces of the AC-A sample before and after PPT showed almost identical topography, in terms of pore depth (before PPT) and pitting (after PPT), see Figures 6 B and C. The average pitting depth reached only 15.6 μm and calculated PF = 1.01 after PPT, typical for general corrosion. The very small value of CR = 0.0058 mm/y and PF = 1.01 for the AC-A sample indicate, that the hard-anodized layer thanks to high stability is valid as a barrier against the influence of the used environment, under set conditions.

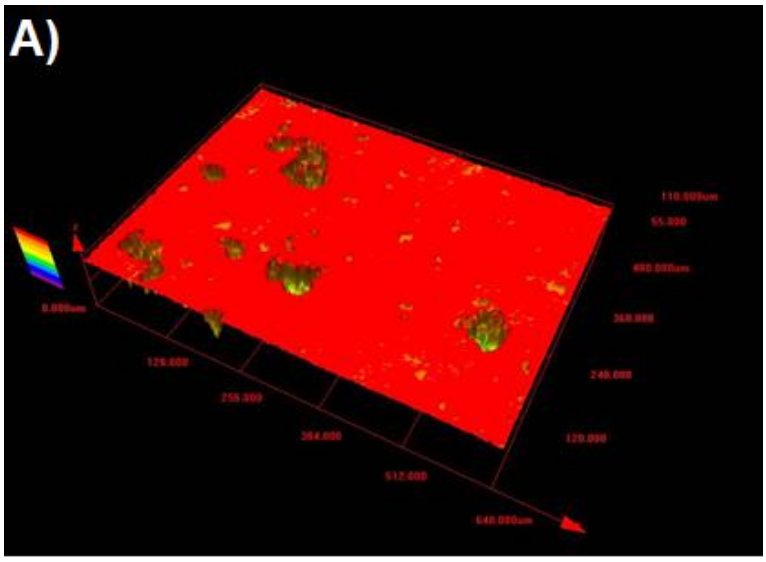

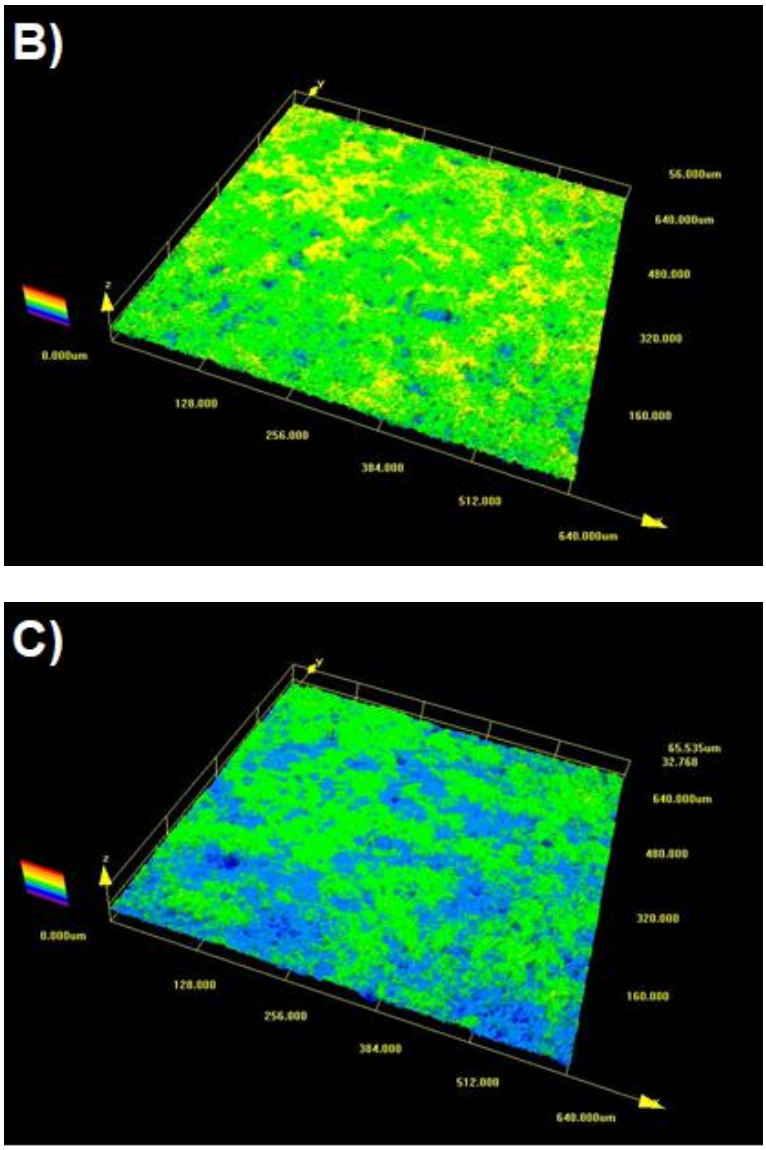

Figure 6. 3D morphology of AC sample (A) and AC-A sample (B) after PPT and AC-A sample before PTT (C), Olympus LEXT OLS 3000, magnification 20x.

Conclusion

The corrosion resistance of artificial aged EN AW 7075 alloy is by intermetallic particles distribution affected, in terms of their chemical composition, density and their size. Intermetallic particles distribution is highly on the heat treatment dependent, so the corrosion resistance too. Part of these intermetallics are polarized anodically ($MgZn_2$, Mg_2Si) or cathodically (Al_7Cu_2Fe, Al_3Fe and Al_2CuMg) to the α solid solution (matrix) having a different interaction with the α solid solution (matrix). Additionally, more complex intermetallics were found in the matrix, based on Al-Fe-Si-Cr-Cu-Mn-Zn elements. For corrosion resistance improvement was the investigated EN AW 7075 T6 alloy hard-anodized and hot-sealed, where a portion of formed intermetallics remained trapped in the hard-anodized layer.

The presence of intermetallics caused increased pitting sensitivity during the PPT with a total corrosion rate of CR = 0.227 mm/y and with calculated PF = 1.36 for the AC sample. However hard-anodized and hot-sealed layer (AC-A sample), shifted E_{corr} (mV) to more positive value E_{corr} = - 202.79 mV, decreased I_{corr} = 0.49 μA, significantly increased polarization resistance R_p = 85 331 Ohm. This beneficial effect, thanks to hard-anodized layer stability, led to reduced corrosion rate CR = 0.006 mm/y and low pitting factor PF = 1.01.

Acknowledgements

The present research work was supported by the projects "VAROPS (DZRO VAROPS FVT3) Military autonomous and robotic systems", "AIROPS (DZRO AIROPS FVT1) Airspace operation", supported by the Ministry of Defence of Czech Republic and by the specific graduate research of the Brno University of Technology No. FEKT-S-20-6206.

References

1. D. Liu, H.V. Atkinson, P. Kapranos, W. Jirattiticharoean, and H. Jones, *Materials Science and Engineering*, **A 361** (2003).
2. S. K. Das, and J. G. Kaufman, in *Aluminum Alloy for Transport, Packing, Aerospace, and Other Application*, pp. 61-72, TMS, Pittsburgh (2007).
3. E. A. Starke, Jr., and J. T. Staley, *Prog. Aerospace Science.*, **32** (1996).
4. W. S. Miller, L. Zhuang, J. Bottema, A. J. Wittebrood, P. De Smet, A. Haszler, and A Vieregge, *Materials Science and Engineering*, **A280** (2000).
5. Alunet. *EN AW 7075 (AlZnMgCu1,5).* 2021, http://www.alunet.cz/ENAW-7075. Accessed 28 June 2021.
6. Y. Liu, J. M. C. Mol, G. C. A. M. Janssen, Journal of Bio- and Tribo-Corrosion, **2 (9)** (2016).
7. J. K. Park, *Materials Science and Engineering:A*, **103 (2**) (1988).
8. I. P. Huang, K. H. Chen, S. Li, and M. Song, *Scripta Materalia*, **56** (2007).
9. J-F. Li, Z-W. Peng, Ch-X. Li, Z-Q. J, W-J Chen, and Z-Q. Zheng, *Trans. Nonferrous Met. Soc. China*, **18** (2008).
10. M. Remešová, S. Tkachenko, D. Kvarda, I. Ročňáková, B. Gollas, M. Menelaou, L. Čelko, and J. Kaiser, *Applied Surface Science*, **315** (2020).
11. G. E. Thompson, G. C. Wood, in *J. C. Scully (Ed) Treatise on Materials Science and Technology*, **23**, Academic Press, London (1983).
12. L. E. Fratila-Apachitei, F. D. Tichelaar, G. E. Thompson, H. Terryn, P. Skeldon, J. Duszczyk, and L. Katgerman, *Electrochimica Ac*ta, **49** (2004).
13. F. Snogan, Ch. Blanc, G. Mankowski, and N. Pébère, *Surface and Coatings Technology*, **154** (2002).
14. M. Shahzad, M. Chaussumier, R. Chieragatti, C. Mabru, and F. Rezai-Aria, Materials and Design, **32** (2011).
15. L. Katgerman, D. Eskin, Hardening, annealing, and ageing, in *Handbook of Aluminum*, G. E. Totten and D. S. MacKenzie, editors, **1**, p. 259–303, Marcel Dekker; USA (2003).
16. A. L. Garcia-Garcia, I. Dominquez-Lopez, L. Lopez-Jimenez, J. D. O. Barceinas-Sanchez, *Materials Characterization*, **87** (2014).
17. M.K.Cavanaugh, R.G. Buchheit, N. Birbilis, *Engineering Fracture Mechanics*, **76** (2009).

18. R. Morgenstern, A. Martin, N. Lehnert, I. Scharf, M. Hackert-Oschätzchen, A. Schubert, and T. Lampke, *IOP Conf. Series: Materials Science and Engineering*, **480** (2019).